Available online at www.sciencedirect.com
ScienceDirect
Continental Shelf Research 29 (2009) 234–251
CONTINENTAL SHELF RESEARCH
www.elsevier.com/locate/csr

The bulge circulation in the Columbia River plume

Alexander R. Horner-Devine

Civil and Environmental Engineering, University of Washington, Seattle, WA 98195, USA

Received 29 January 2007; received in revised form 15 December 2007; accepted 19 December 2007
Available online 31 December 2007

Abstract

While most numerical and laboratory models of coastal river inflows result in the generation of a large anticyclonic bulge near the mouth of the river, evidence of such a feature in field observations is scant. Here, results from a series of approximately shore-parallel transects 20 km west of the mouth of the Columbia River are presented that provide a detailed description of the bulge circulation in the plume during a period of moderate wind stress. The transect data include velocity and density measurements in the upper 30 m of the water column, acquired with a vessel-mounted ADCP and a CTD towed on a vertically undulating TRIAXUS towfish, respectively. Sampling spanned more than 19 h of the mixed semidiurnal tidal cycle, and the anticyclonic circulation persisted throughout this period. The core of the bulge circulation, defined as the central region where the azimuthal velocity varies linearly, is approximately 5 m deep and 22 km in diameter, and the entire bulge circulation is 30–40 km in diameter. The observations from the Columbia plume agree well with the structure and scales proposed in laboratory and numerical model studies. The existence of the core region of constant vorticity agrees with laboratory studies that also show the bulge to be in solid-body rotation. The average rotation rate in this region is approximately $-0.8f$, close to the zero potential vorticity limit. Estimates of each of the terms in the radial momentum equation confirm that the bulge is in gradient-wind balance. Predictions based on previous analytical and scaling theories and observations from the Columbia plume suggest that the accumulation of freshwater in the bulge should reduce the northward coastal current flux to approximately 35% of the river discharge. This agrees with preliminary estimates of northward flux in the coastal current during the same period.

Keywords: River plume; Transport; Columbia River; Bulge circulation

1. Introduction

River inputs to coastal waters contribute terrigenous nutrients, sediments and contaminants, all of which can have profound impacts on sensitive coastal ecosystems (Jickells, 1998). In addition, the coastal plume formed by the buoyant inflow constitutes an important dynamical component of the coastal circulation. Due to their ecological and dynamical importance, a good understanding of the mixing and transport processes in river plumes is required for the maintenance of coastal ecosystems and their resources.

Until relatively recently, coastal models commonly assumed that buoyant water entering the coastal ocean from medium and large-scale rivers was deflected immediately to the right (left) in the Northern (Southern) hemisphere and transported away from the river mouth in the coastal current. This implies that all of the river water is transported by the coastal current and the plume is steady. As described in Section 2, research over the last 10–20 years suggests that this simple model may not be valid in many cases. In particular, laboratory and numerical model studies of river plumes result in a constantly growing anticyclonic eddy, or "bulge", near the river mouth, which reduces the flux of river water away from the mouth by approximately 25–70%. As a consequence of the reduced flux, the effective residence time of water in the bulge may be a few days. This may be associated with elevated chlorophyll *a* (Horner-Devine et al., 2008), primary productivity (Kudela et al., 2006) and low dissolved oxygen in some systems (Schofield et al., 2007).

The bulge in the Columbia River plume is shown in Fig. 1a as observed from the MODIS satellite on June 9, 2005, the first day of *in situ* sampling described in this paper. Due to hazy atmospheric conditions, the plume

E-mail address: arhd@u.washington.edu

0278-4343/$ - see front matter © 2008 Elsevier Ltd. All rights reserved.
doi:10.1016/j.csr.2007.12.012

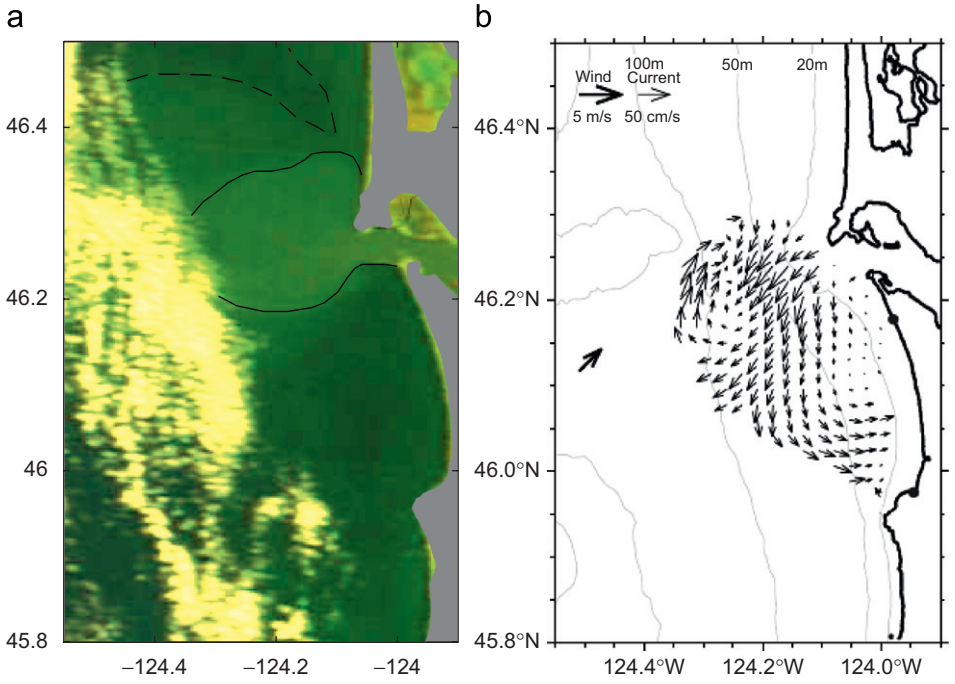

Fig. 1. Remote sensing of the Columbia River plume. (a) Modified truecolor image from the MODIS satellite from June 9, 2005. The solid line outlines plume water in the bulge and the dashed line outlines more dilute plume water. The bright region in the left side of the image is due to cloud cover. This image is courtesy of Raphael Kudela (UCSC). (b) Velocity vectors derived from radar for 12:00 on June 10, 2005 showing an anticyclonic circulation centered at 124.25°E and 46.2°N. The single bold vector shows the wind direction and magnitude. This image is courtesy of Mike Kosro, OSU.

water is somewhat difficult to distinguish from ambient ocean water in the image and an approximate bulge boundary has been added (solid line) to help differentiate it. The bulge is the roughly circular mass of water marked by brighter sea surface color directly offshore of the river mouth. Although the exact relationship between sea surface color, which is presumably due to fine suspended sediment and organic matter, and salinity is not known, the satellite image provides a valuable qualitative picture of the plume shape (e.g. Thomas and Weatherbee, 2006). The anticyclonic circulation within the bulge is captured in radar measurements of surface velocity on June 10, 2005, the second day of *in situ* sampling (Fig. 1b). The center of the circulation appears further south in the radar measurements than the MODIS image, consistent with observations in this paper that the circulation shifts south during this period. The estuary discharge also appears to generate a cyclonic eddy in the coastal water south of the river mouth. This eddy may be associated with return flow into the estuary, which has been observed to be concentrated on the south side of the estuary.

This work presents field observations of the bulge circulation in the Columbia River plume on the Washington-Oregon coast and compares these observations to theoretical, laboratory and numerical model results.

2. Background

Chao and Boicourt (1986) used the term "bulge" to describe the transition region separating the initial estuarine outflow from the bore-like coastal current that forms downstream (in the sense of Kelvin wave propagation) due to the Earth's rotation. According to their numerical model experiments, the bulge is a non-linear region whose expansion is determined by the ratio of the gravity current propagation speed within the estuary and that along the coast. The bulge generally expands offshore because mixing within the bulge lowers the coastal propagation speed relative to the estuarine propagation speed. Most numerical model experiments also reproduce this anticyclonic non-linear circulation near the river or estuary mouth (e.g. Oey and Mellor, 1993; Kourafalou et al., 1996; Garvine, 2001; Fong and Geyer, 2002). Many impose an ambient current in the same direction as the coastal current (e.g. Garvine, 1987), which augments the alongshore transport in the plume, arrests the offshore expansion of the bulge, and causes the plume to be steady (Fong and Geyer, 2002). The steady bulge circulation is considered analytically in Yankovsky and Chapman (1997). For plumes that are detached from the bottom, they assume that the bulge momentum is characterized by a gradient-wind balance and derive a length scale that characterizes the radius of the bulge circulation. Laboratory experiments confirm that their assumed momentum balance is correct, however, the assumption of steadiness may not be valid in many cases (Horner-Devine et al., 2006).

In a series of numerical model experiments Fong and Geyer (2002) show that the alongshore freshwater transport is reduced to 25–70% of the river discharge as a result

of the continual growth of the bulge region. They relate the alongshore transport in the plume to the Rossby number associated with the river inflow into the coastal ocean, $Ro_i = U/fW$, where U, W and f are the mean velocity and width of the river inflow, and the Coriolis parameter, respectively. In their model runs, the bulge was pressed close to the coast, and the alongshore transport was high for low Ro_i. This description of the dynamics agrees with the analytical model of Nof (1988), who suggests that the along-wall flux of buoyant fluid escaping from an eddy is a function of the fraction of the eddy that is "clipped" by the wall.

Pichevin and Nof (1997) investigate the momentum balance in buoyant oceanic inflows for the case when the inflow velocity is perpendicular to the coast using a two-layer analytical model. They show that, in the case of a steady inflow, no force exists to balance the flux of momentum away from the mouth in the coastal current. In a subsequent paper, Nof and Pichevin (2001) suggest that this apparent paradox is resolved if the bulge is allowed to expand offshore. For this unsteady plume, the offshore expansion of the bulge contributes a Coriolis force that opposes the coastal current momentum flux.

Recent laboratory experiments also confirm the existence of an unsteady bulge. Avicola and Huq (2003) use a scaled estuary discharge on a rotating table and reproduce an unsteady, anticyclonic bulge circulation similar to that observed in the numerical model experiments. They scale the bulge depth using a geostrophic scale based on the inflow discharge Q, $h_b = (2Qf/g')^{1/2}$, and the bulge width using an internal Rossby radius for the bulge based on the geostrophic depth, $L_b = (2Qg'/f^3)^{1/4}$. Where $g' \equiv \Delta\rho/\rho_0$ is the reduced gravity.

Horner-Devine et al. (2006), referred to hereafter as HD06, simulate the river plume in the laboratory with a direct inflow condition, resulting in a larger range of inflow Froude numbers ($Fr_i = U/(g'H)^{1/2}$). Here H refers to the thickness of the inflow. These experiments agree with the scaling for the bulge depth and radius presented by Avicola and Huq (2003), but introduce a second length scale to describe the bulge dynamics. HD06 find that the center of rotation of the anticyclonic circulation in the bulge is displaced from the coast by a distance that scales with the inertial radius, $L_i = U/f$. Thus, the dynamics of the bulge depend on the bulge radius r_b and the offshore displacement of the bulge center y_c. Although both r_b and y_c increase with time, they scale with the internal Rossby radius and inertial radius, respectively, which are constant in time. In other words, $r_b = \varepsilon_r(t)L_b$ and $y_c = \varepsilon_y(t)L_i$, where ε_r and ε_y are functions of time describing the bulge growth (see HD06). The degree to which the bulge is pressed against the coast depends on the ratio of the two length scales, $L^* = L_i/L_b$. If $L^* \ll 1$, the bulge is pressed close to the coast relative to its radius and a large fraction of the river discharge flows away from the river mouth in the coastal current. When $L^* \to 1$, the bulge is forced offshore by the strength of the river inflow, retaining a large fraction of the discharge, and causing relatively less freshwater to flow away in the coastal current. Measurements of the coastal current flux in HD06 and Fong and Geyer (2002) agree with the above theory and predict that the accumulation of freshwater in the bulge scales according to Ro_i^n, where $0.17 < n < 0.32$ is an experimentally derived exponent. The experiments in HD06 also confirm the assumption made by Yankovsky and Chapman (1997) that the bulge momentum is in gradient-wind balance. Note that the observation that the bulge is in gradient-wind balance appears to conflict with the finding that the bulge grows continuously since the gradient-wind balance assumes the flow is steady. This apparent contradiction is resolved in Section 3, where it is shown that the contribution from the bulge growth is negligible in the momentum balance except in the initial 1–2 days spin-up of the bulge.

The above results lead to a simple conceptual model relating the bulge dynamics to the alongshore freshwater flux. When the bulge is displaced from the coast by a distance close to its radius ($L^* \to 1$), the anticyclonic circulation is nearly symmetric and the net shore-directed Coriolis force is small. Since this is the only force available to press the bulge against the coast, it maintains its position offshore. Whitehead (1985) described the dynamics of a coastal jet in terms of the angle of incidence that it makes with the wall upon its re-attachment. He showed that the transport into the coastal current was greatest for small angles, decreased as the angle approached 90° (normal to the coast) and approached zero as the angle increased significantly beyond 90° (directed back upstream). When L^* approaches 1, the angle of incidence of the recirculating bulge flow is greater than 90°, and the majority of the impinging fluid is directed back into the bulge. By contrast, when the bulge is held close to shore, the returning bulge flow is clipped, the integrated Coriolis force is relatively larger, the incidence angle is small and the flux of buoyant fluid into the coastal current is large. The above model does not clearly establish a causative relationship, since the distance from shore and cross-shore force are interrelated. The results presented in HD06, however, suggests that the inflow velocity U sets the location of the bulge initially, and determines the subsequent dynamics of the bulge.

Despite the fact that the bulge is observed consistently in laboratory and numerical models of river plumes, there remains scant evidence of the bulge from field observations. This led Garvine (2001) to suggest that the bulge may be an artifact of how models are configured. In particular, he suggests that the simple rectangular inlet is suspect and that models should be modified to account for a reduced coastal wall, estuary-like inflow and a non-zero inflow angle. He presents evidence from observations and model runs of the Delaware River plume that support his conclusions. Recent results, however, show that a bulge forms under certain conditions in the Hudson River plume and reduces the alongshore freshwater flux to approximately 1/3 to 1/2 of the discharge (Chant et al., 2008).

The Columbia River plume has also been observed to form a bulge-like circulation (Hickey et al., 1998). Since the bathymetry is steep and the estuary mouth is relatively narrow, it meets the criteria for which the bulge may form suggested by Garvine (2001). In this work, we present field observations of an anticyclonic bulge circulation in the Columbia plume during a period of moderate wind stress.

3. Theory

In this section, a theoretical interface profile $h(r)$ and the instantaneous bulge volume V_b are derived for a two-layer gyre with constant vorticity following a similar derivation in Nof (1981). The equation for the two-layer frictionless radial momentum balance in a buoyant lens is (e.g. Flierl, 1979; Nof, 1981)

$$\frac{\partial u_r}{\partial t}+u_r\frac{\partial u_r}{\partial r}+\frac{u_\theta}{r}\frac{\partial u_r}{\partial \theta}-\frac{u_\theta^2}{r}-fu_\theta=-g'\frac{\partial h}{\partial r}. \tag{1}$$

Here, u_r and u_θ are the depth-averaged radial and azimuthal velocity, respectively, r and θ are the radial and azimuthal coordinates, respectively, and h is the plume thickness. Yankovsky and Chapman (1997) proposed that the radial momentum balance for river plume bulges is the gradient-wind balance

$$\frac{u_\theta^2}{r}+fu_\theta=g'\frac{\partial h}{\partial r}. \tag{2}$$

Note that this balance is referred to as a cyclostrophic balance in Yankovsky and Chapman (1997). In order for Eq. (1) to be reduced to Eq. (2), the first three terms must be small relative to the final three. This is not immediately obvious since the bulge observed in laboratory and numerical model experiments expands continuously. Thus, the flow cannot be considered steady and u_r cannot be considered equal to zero *a priori*. In the following analysis, it will be shown that the first two terms, which are non-zero due to the bulge expansion, are nonetheless small relative to the terms in Eq. (2) if the radius of the bulge is large. Thus, the bulge maintains a momentum balance dominated by the gradient-wind terms, despite the fact that it is slowly expanding. The third term is also assumed small since the flow is radially symmetric. We will proceed by assuming that the flow is described by Eq. (2) and subsequently estimate the magnitude of the first two terms in Eq. (1) resulting from the volumetric expansion of the bulge.

For the purposes of this analysis, we consider the case corresponding to solid-body rotation with non-zero potential vorticity and define an average bulge vorticity as

$$\omega_b=\frac{2u_\theta}{r}. \tag{3}$$

The assumption of solid-body rotation was verified in the laboratory experiments of HD06, who found that the azimuthal velocity varied linearly with the radius throughout the central region of the bulge. We refer to this region as the core of the bulge.

Substituting ω_b into Eq. (2) and integrating radially from 0 to r gives

$$h(r)-h(0)=\frac{\omega_b\left(\frac{\omega_b}{2}+f\right)}{2g'}\frac{r^2}{2}. \tag{4}$$

The edge of the bulge is defined as $r=R$ and the interface is assumed to surface at the edge so that $h(R)=0$. Using this condition, the radial interface profile is

$$h(r)=\frac{\omega_b\left(\frac{\omega_b}{2}+f\right)}{4g'}(r^2-R^2). \tag{5}$$

Eq. (5) depends on ω_b and R, which are not known *a priori*. If the bulge is assumed to have zero potential vorticity ($\omega_b=-f$), Eq. (5) simplifies further to

$$h(r)=-\frac{f^2}{8g'}(r^2-R^2), \tag{6}$$

which depends solely on the outer radius, R. Eqs. (5) and (6) will be compared with observations from the Columbia plume in Section 5.

Integrating $h(r)$ over the radius, the bulge volume is found to be

$$V_b(R,t)=2\pi\int_0^R h(r)r\,\mathrm{d}r=\frac{\pi f^2}{16g'}R^4. \tag{7}$$

The zero potential vorticity case is used here and for the remainder of the analysis for simplicity, although the extension to the constant vorticity case is straightforward.

In order to evaluate the magnitude of the first two momentum terms in Eq. (1), consider a bulge that accumulates a constant fraction of the river discharge, βQ. This is consistent with the observations in HD06 and Fong and Geyer (2002) that the transport of freshwater in the coastal current is constant after 2–3 days. The rate of change of the bulge volume $\partial V_b/\partial t$ must be equal to the rate of accumulation of water in the bulge

$$\beta Q=\frac{\pi f^2}{4g'}R^3\frac{\mathrm{d}R}{\mathrm{d}t}. \tag{8}$$

Thus, the radial velocity due to a constant increase in bulge volume is

$$u_r=\frac{\mathrm{d}R}{\mathrm{d}t}=\frac{4\beta Qg'}{\pi f^2R^3} \tag{9}$$

and the acceleration is

$$\frac{\partial u_r}{\partial t}=-\frac{3}{R^7}\left(\frac{4\beta Qg'}{\pi f^2}\right)^2. \tag{10}$$

The form of the radial velocity, Eq. (9), is the same as the gyre migration speed determined by Nof and Pichevin (2001). The constants differ, however, since the present analysis assumes constant freshwater transport in the coastal current, whereas Nof and Pichevin (2001) invoke a momentum argument to close the balance. It can

be shown that the radial advective acceleration $u_r \partial u_r/\partial r$ is also equal to $-3/R^7(4\beta Q g'/\pi f^2)^2$.

According to HD06 and Fong and Geyer (2002), $0.25<\beta<0.70$. For the purposes of this analysis the bulge will be assumed to accumulate half of the river discharge, i.e. $\beta = 0.5$. For the Columbia plume bulge, $Q \simeq 7000\ \mathrm{m^3\,s^{-1}}$, $g' \simeq 0.1\ \mathrm{m\,s^{-2}}$ and $f = 1\times10^{-4}\ \mathrm{s^{-1}}$. Finally, R is at least 10 000 m. With these values, Eq. (10) gives an estimate of the radial acceleration

$$\frac{\partial u_r}{\partial t} \simeq 6\times10^{-7}\ \mathrm{m\,s^{-2}}. \tag{11}$$

For comparison, the magnitude of the Coriolis term in Eq. (2) can be approximated by $u_\theta f \simeq f^2 R/2$ for a zero potential vorticity eddy. With the above values for f and R, this gives

$$u_\theta f \simeq 5\times10^{-5}\ \mathrm{m\,s^{-2}}. \tag{12}$$

The magnitude of the centripetal term in Eq. (2) is $u_\theta^2/r \simeq f^2 R/4 \sim O(u_\theta f)$ and the pressure term will be on the same order of magnitude as well. Thus, the expansion of the bulge leads to radial and advective acceleration terms that are two orders of magnitude smaller than the terms of the gradient-wind balance. Based on this, the gradient-wind balance is expected to apply even for a growing bulge, as long as the radius is sufficiently large.

This result can be generalized by assuming that the radius scales with the internal Rossby radius (Section 2), $R = \varepsilon_r(t) L_b$. Substituting this into Eq. (10), the ratio of the radial acceleration to the Coriolis term is

$$\frac{\partial u_r}{\partial t}\frac{1}{u_\theta f} = -\frac{24\beta^2}{\pi^2}\frac{1}{\varepsilon(t)^8}. \tag{13}$$

The ratio of unsteady to Coriolis terms is $O(10^{-1})$ when $\varepsilon(t)=1$, but $O(10^{-3})$ when $\varepsilon(t)>2$. In the experiments of HD06 and Avicola and Huq (2003) $\varepsilon(t)>2$ after 1–2 days. Thus, although the radial acceleration associated with bulge growth is an important contribution to the radial momentum balance initially, it is negligible after 1–2 days. After this initial period, the bulge is expected to maintain a quasi-steady momentum balance involving only the terms in the gradient-wind balance.

4. Field observations and conditions

An extensive field investigation of the Columbia River plume was carried out as part of the River Influences on Shelf Ecosystems (RISE) project during 2004–2006. The goal of the RISE project is to understand the impact of the Columbia plume on the coastal ecosystem and, in particular, coastal productivity. The RISE observational effort consisted of four cruises, each with two vessels, the R/V Pt Sur and the R/V Wecoma, which made measurements of the physical, biological and chemical properties of the plume, estuary and surrounding coastal waters. The observations and analyses considered in this work focus on measurements acquired by the R/V Pt Sur during the June 2005 cruise.

4.1. Study site

The Columbia River flows into the Pacific ocean at the Oregon-Washington border through a narrow estuary that is oriented approximately east–west. The buoyant inflow from the estuary generates a large persistent plume on the northwest shelf of the United States, often extending from south of the river mouth to the Canada–US border (Hickey et al., 1998). Near the mouth, the plume is very dynamic, forced by river discharge between 6000 and $15,000\ \mathrm{m^3\,s^{-1}}$ and moderately large tides of up to 4 m that generate currents in excess of $1\ \mathrm{m\,s^{-1}}$. Due to the narrow mouth (3 km) and relatively steep, narrow shelf, the outflow from the estuary typically forms a surface-advected plume that separates from the coast and initially propagates directly west. On the shelf, the plume is strongly stratified and generally limited to the upper 5–10 m of the water column. It is very sensitive to wind conditions, which can cause it to focus into a narrow northward coastal plume during downwelling conditions or a south-westward directed offshore plume during upwelling conditions (Hickey et al., 2005).

The plume is strongly modified by tides in the vicinity of the mouth. On the ebb tide, a pulse of brackish water is discharged from the estuary and forms a thin, stratified plume that rides overtop of existing plume water on the shelf. This plume, which is referred to as the tidal plume, is often bounded by very strong fronts (Orton and Jay, 2005) that may release solitons as the ebb slackens (Nash and Moum, 2005). During the period that is the focus of the present study, the tidal plume was observed to propagate as a thin surface layer across a subtidal re-circulating plume. A description of the tidal and re-circulating plumes during this period is presented as part of a conceptual model of the Columbia plume in Horner-Devine et al. (2008). In the present work we focus on the dynamics of the re-circulating plume, or bulge.

4.2. Instrumentation and measurements

For the June 2005 cruise, the R/V Pt Sur was configured to acquire profiles of horizontal velocity in the upper 2–20 m of the water column using a side-mounted 1200 kHz acoustic doppler current profiler (ADCP). The plume is typically between 5 and 10 m thick, and so the sampling captured most of the plume. The remainder of the instrumentation was carried on TRIAXUS, a towed vehicle with powered flaps that was programmed to undulate behind the vessel and outside of the wake at speeds of up to 7 knots. In its typical sampling mode, TRIAXUS undulated constantly between 2 and 30 m depth and had a repeat time of approximately 2 min for its dives. TRIAXUS carried a large array of instruments for sampling temperature, salinity, depth, particle size and concentration, plankton

abundance and nutrients. For the present work, we focus on the CTD (salinity, temperature and depth) data acquired with a Seabird instrument. After quality control, ADCP data were binned into 20 s bins (approximately 60 m) to get rid of high frequency variability. The TRIAXUS CTD data were sorted into separate casts in order to generate contour maps of the plume salinity.

During the June 2005 cruise, a number of transects were repeated that intersect the plume bulge, and the anticyclonic circulation was observed much of the time. For the purposes of the present work, primarily data acquired on transect Line B are examined in detail (Fig. 2a). This line runs exactly north–south, is located 20 km offshore of the mouth of the Columbia River and is centered slightly north of the river mouth. The estuary discharge, which is directed due west during maximum ebb, intersects the southern half of the transect line. Six transects on Line B were carried out starting at 17:30 h GMT on June 9 and ending at 12:45 on June 10, covering a total of 19.2 h. The high tide prior to maximum ebb occurred at 9:50 on June 9. However, as discussed in Section 5.4, the dominant tidal influence on the bulge is due to the estuary discharge, which is subject to a lag of approximately 3 h. When this lag is accounted for, the first transect begins 4.7 h after high tide and, thus, shortly after maximum ebb.

The TRIAXUS is a valuable platform for plume studies as it permits sampling close to the surface at relatively high vessel speeds. In the region surrounding the mouth of the Columbia River, however, the TRIAXUS was very susceptible to snags on crab pots, which often required lengthy repairs on deck. This occurred in the middle of the transecting described herein and resulted in the loss of CTD data for one fifth of the fourth transect and all of the fifth and sixth transects.

4.3. Conditions

The peak river discharge in the spring of 2005 occurred on May 20, 18 days prior to the sampling described here. On June 9–10, the average discharge was approximately 7000 $m^3 s^{-1}$ (Fig. 2b). The sampling on Line B came at the end of a 4 day period during which the winds were moderate and their direction was variable (Fig. 2c). The variability of the winds resulted in conditions that were not conducive to either upwelling or downwelling during the study period. Winds were persistent from the Northwest for a 4–5 day period at the beginning of the month. Under such upwelling conditions, the plume is typically directed offshore and northward transport is low (Hickey et al., 2005). The observed plume behavior, therefore, appears to have commenced 3–4 days prior to the sampling period. Tides in the vicinity of the Columbia plume are mixed semidiurnal and have amplitudes in the range of 2–4 m. The sampling was 4 days after spring tide.

5. Results

5.1. Plume structure and volume

The velocity and salinity structure of the bulge circulation is presented in Fig. 3 for Transect 3 on Line B (see Fig. 2) 14.7 h after high tide. This transect captures the entire circulation, although there appears to be some additional buoyant water to the south. In Fig. 3, the distance along the transect is shown relative to the center of rotation of the circulation, which is 46°25′N for this transect. The methodology for computing the location of the center is described later in Section 5.2.

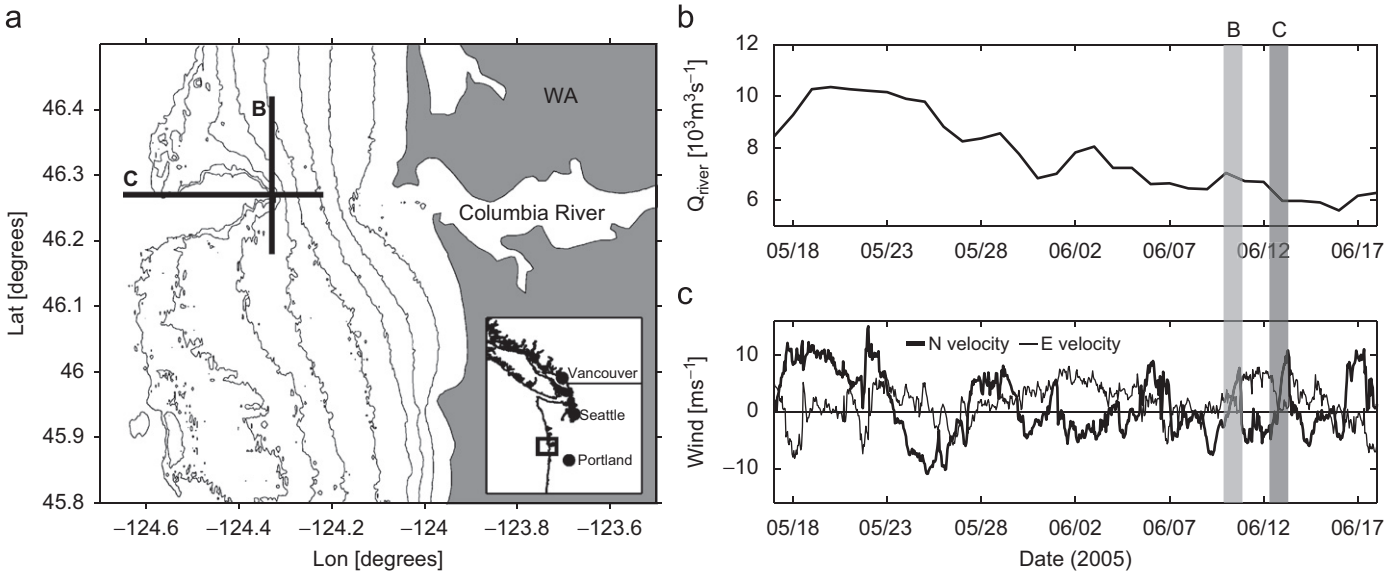

Fig. 2. (a) Transect Lines B and C location (thick line) relative to the mouth of the Columbia River. The map location is shown in the inset and contour lines are isobaths spaced at 50 m. (b) Columbia River discharge measured by the USGS at the Beaver Army Terminal, Quicy, OR. (c) North and East wind velocity components from NOAA buoy 46029, located near the mouth of the Columbia River.

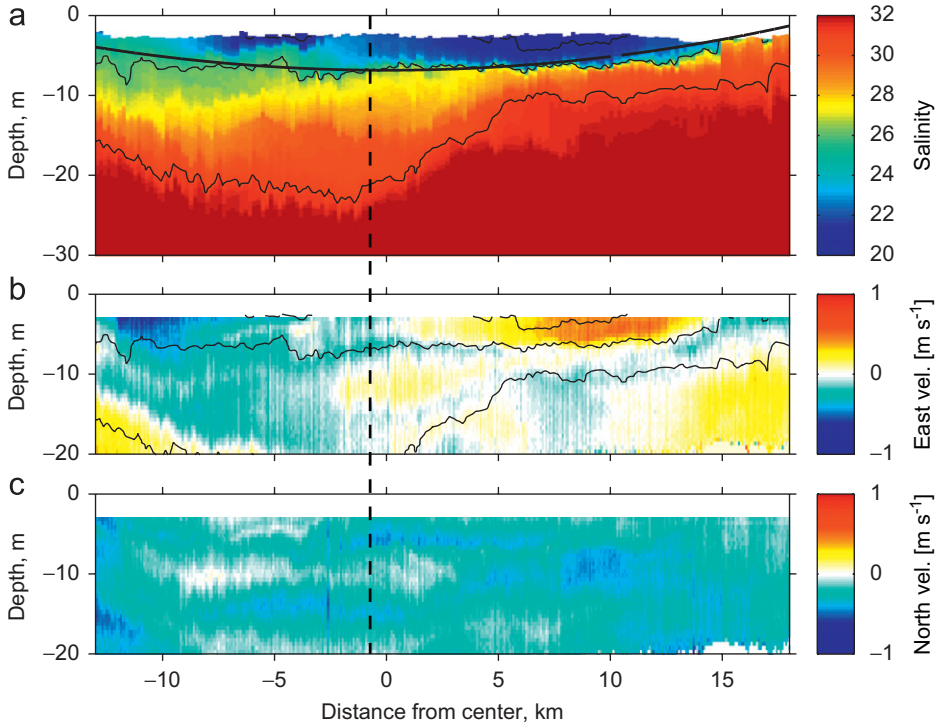

Fig. 3. Structure of the bulge circulation and buoyancy 14.7 h after high tide. (a) Salinity cross section from the TRIAXUS CTD. The thin black lines are salinity contours with values of 21, 26 and 31, from shallowest to deepest. The thick black dashed line is the theoretical interface profiles assuming constant potential vorticity (Eq. (5)). (b) and (c) East and North velocity field, respectively, measured with the side-mounted 1200 Hz ADCP. The transect runs south to north and the x-axis in each panel is the distance from the center of rotation (46°25′N, 124°20′E). Negative (positive) distances (r) correspond to locations south (north) of the center of rotation. The salinity contours in (a) are reproduced in (b) for comparison of the plume structure. The vertical dashed line indicates the latitude of the estuary outflow.

While the surface layer is warmer than the deeper ocean water, the buoyancy is due primarily to the salinity anomaly. The average salinity in the near-surface layer is approximately 23 and the temperature, is 15 °C, approximately 5 °C higher than the deeper ocean water. It appears that the temperature anomaly is due to a combination of surface warming and river input, since it extends beyond the salinity anomaly in the surface layer (not shown). Qualitatively, we observe a 5–10 m deep lens of buoyant water with westward velocity on the south end and eastward velocity on the north.

Transects 1, 2 and 4 show a similar overall structure to Transect 3 (not shown). In Transects 1 and 2, however, the structure of the plume near the northern front is modified by the passage of internal waves released from the tidal plume. These transects are presented and the propagation of the internal wave packet is discussed in Horner-Devine et al. (2008). Equipment problems prevented the use of the TRIAXUS for approximately one fifth of Transect 4 and all of Transects 5 and 6. While we were not able to measure vertical salinity structure for this period, ADCP velocity and surface salinity/density were still acquired.

While the freshest plume water forms a symmetric parabolic lens (see Section 5.5) near the surface, the vertical structure below the plume differs to the south and north. To the south, low salinity water extends down to 22 m depth (Fig. 4a). The water column is divided into two stratified sections (Fig. 4b). Stratification is high above 5 m depth, with buoyancy frequency $N = 0.025\,\mathrm{s}^{-1}$, and lower between 5 and 25 m, with $N = 0.015\,\mathrm{s}^{-1}$. Here, $N^2 \equiv -(g/\rho_0)\,\mathrm{d}\rho/\mathrm{d}z$. North of the center of rotation the plume base is much more strongly stratified, with $N = 0.06\,\mathrm{s}^{-1}$ at $z = -5.5$ m, and the water column is relatively well mixed above and below the interface (Figs. 4a and b).

The north–south asymmetry in vertical structure is apparent in all transects through the bulge, and is likely the result of increased mixing on the south side of the bulge due to the energetic estuary inflow. Horner-Devine et al. (2008) estimate that the eddy diffusivity in the westward flow is more than 25 times that of the returning eastward flow. The bulge becomes less stratified and the water column approaches a two-layer system as the plume fluid flows anticyclonically from south to north. The fate of the intermediate salinity fluid generated near the river mouth and observed on the south side of the bulge cannot be determined from the data considered here. However, satellite images often show patches of plume water south of the bulge during periods of northward plume flow. It is possible that the intermediate salinity fluid escapes from the bulge and is advected to the south by the regional coastal current flowing beneath the plume circulation. ADCP data indicate that the flow beneath the plume is southward in most of the transects considered here. Further analysis of this transport mechanism is beyond

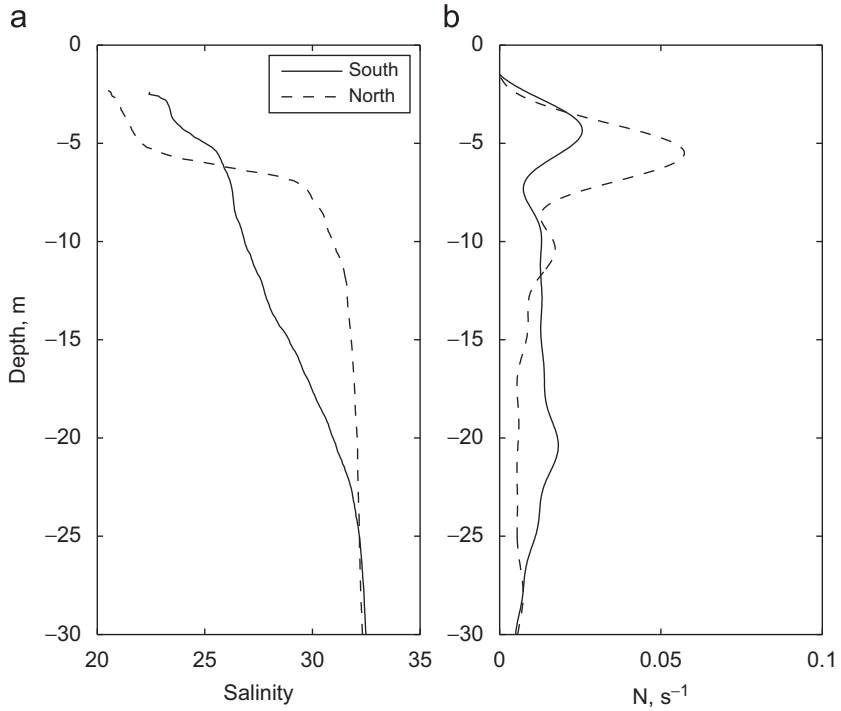

Fig. 4. Vertical profiles of (a) salinity and (b) buoyancy frequency. Each plotted profile is the average of 18 profiles from the TRIAXUS CTD spanning a north–south distance of 3.3 km. The two profiles correspond to westward-flowing plume water south (solid line) of the center of rotation and eastward-flowing water to the north (dashed line). The averages are each centered 9.5 km south and north of the center of rotation, respectively.

the scope of the present work and is left for further investigation.

Due to the difficulty in identifying a distinct interface south of the center of rotation, the plume depth is determined based on the isohaline with salinity of 26. This corresponds roughly to the observed maxima in the vertical salinity gradient. During the four passes in which TRIAXUS data were acquired, the average plume depth near the center of the bulge varied between 6.6 and 10.2 m (Fig. 5a). The plume density, defined as the average of the density measurements in $S<26$ water, is $1015.8\pm 0.07\,\mathrm{kg\,m^{-3}}$. This estimate is biased high since the TRIAXUS does not sample the freshest water in the top 1–2 m of the water column. Based on the average plume density the effective reduced gravity is $g' = 0.097\,\mathrm{m\,s^{-2}}$, where a reference density of $1026\,\mathrm{m^{-3}}$ is used.

The two-dimensional salinity field observed along this transect can also be used to estimate the freshwater volume of the bulge by assuming that the bulge is circular. This assumption is justified, for example, in satellite images such as the one shown in Fig. 1a. The equivalent freshwater volume is calculated by integrating the observed salinity field according to

$$V_{fw} = \int_0^{\pi}\int_0^{-H}\int_0^{R}\frac{\Delta S}{S_0}\,\mathrm{d}r\,\mathrm{d}z\,\mathrm{d}\theta. \tag{14}$$

Here H is the maximum measurement depth (>30 m), which exceeded the depth of the salinity anomaly in all cases. r is the radial coordinate relative to the center of rotation (see Section 5.2) and R is the maximum radius of the bulge defined as the location at which the velocity returns to zero. Since the endpoints of the transect generally extended beyond the edge of the bulge, the entire transect was included in the integration. The salinity anomaly is defined as $\Delta S \equiv S_0 - S$, where the reference salinity is $S_0 = 32$. The salinity in the unresolved surface layer was estimated based on the vessel's underway salinity measurement and, alternately, by assuming a constant salinity above the uppermost TRIAXUS measurement. These are conservative estimates of the freshwater content. The two techniques resulted in estimates that differed by approximately 4%.

In Fig. 5b the equivalent freshwater volume for Transects 1–4 is normalized by the daily volumetric freshwater flux from the river, QT, where T is 1 day. The bulge volume varies between 3.3 and $3.9QT$. This observed freshwater volume is an important result, as it confirms that the bulge has accumulated river water over the course of the preceeding 3–4 days. In fact, most laboratory and numerical model experiments predict that the bulge retains approximately 50% of the river inflow, which implies that 6–8 days worth of accumulation may be in the bulge.

5.2. Surface velocity and salinity

The surface velocity is obtained by averaging the uppermost 5 bins in the ADCP record, which corresponds to a layer from 3.0 to 5.5 m depth (Figs. 6a–f). The structure of the surface velocity profile is relatively insensitive to the chosen averaging depth. It is clear from

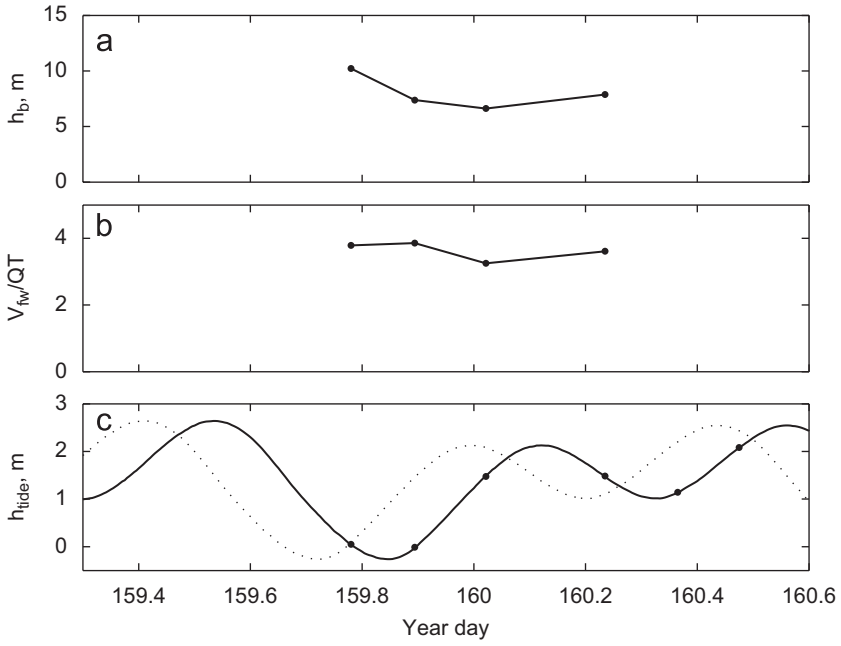

Fig. 5. Temporal variability of the bulge. (a) Mean bulge depth based on the $S = 26$ isohaline. (b) Freshwater volume of the bulge normalized by QT, the daily freshwater discharge from the Columbia River. (c) Tidal elevations at the mouth of the Columbia River (dotted line) and tidal elevations shifted by 3 h to account for the travel time between the mouth and the transect location (solid line). In each panel, dots correspond to the average time of each transect.

Figs. 6a–f that the anticyclonic circulation persists throughout the tidal cycle.

The core of the anticyclonic circulation is identified as the region between the locations of maximum westward (negative) and eastward (positive) velocity in the surface profile. The observed velocities in the core region were fit to a linear profile. The linear fit explains between 94% and 98% of the variability in each of the six passes, confirming the assumption that the bulge velocity is in solid-body rotation. The center of rotation is determined from the linear fit, based on the location of zero velocity. In Figs. 6a–f, the surface velocity profile for each pass is plotted versus the distance from the center of rotation, r. During the sampling, the center of rotation moved approximately 10 km to the south (Fig. 8a). For this reason, the final three transects did not capture the westward velocity maximum. For these transects the southern-most velocity measurement is used to define the southern extent of the core for the purposes of the above analyses.

A composite velocity profile is computed by averaging the velocity from each pass in radial bins (Fig. 6m). The tidal signal in the region of the Columbia plume is complex due to strong baroclinic tides and full tidal correction is beyond the scope of this work. The composite profile spans a period of 18 h, starting shortly after greater ebb and ending 1 h into the subsequent greater ebb, and is considered to be an approximation to the subtidal surface velocity profile in the bulge. It should be noted that the averaging breaks down on the southern end of the profile. The bulge is slightly distorted and translated during the first three passes, presumably due to local winds. This results in a double-peaked shape in the westward velocity, which is an artifact of the averaging.

Corresponding surface salinity profiles from the vessel's underway CTD are plotted in Figs. 6g–l. Here the radius is determined from the center of rotation as above. Fronts that propagate northward across the bulge can be seen in the surface salinity profile and are discussed in more detail in Horner-Devine et al. (2008). A composite surface salinity profile is computed in the same manner as the velocity profile (Fig. 6n).

Assuming that the bulge circulation is radially symmetric, representative velocity, length and vorticity scales can be inferred from the surface velocity and salinity profiles in Figs. 6m and n. The radius of the constant vorticity core r_c is 11 km, and is symmetric about the center of rotation, although the data south of the center is subject to the averaging errors mentioned above. The maximum westward velocity is $0.5\,\mathrm{m\,s^{-1}}$, slightly higher than the maximum returning velocity of $0.45\,\mathrm{m\,s^{-1}}$.

Although the velocity maximum occurs at $r_c = 11$ km, the northern extent of the bulge r_b is much larger. Based on the location of zero velocity and decreased surface salinity gradient, $r_b = 20$ km. Although the surface salinity does not reach that of the ambient ocean at this point, the structure of the density field confirms that this is an appropriate scale for the edge of the bulge (Fig. 3a). It is worth noting here that the theory presented in Section 3 and that of Nof (1981) and Flierl (1979) assumes that the interface surfaces at R, the location of the maximum velocity. The current data suggest the radius based on the maximum velocity is significantly smaller than the radius

where the interface surfaces. This is discussed in more detail in Section 6.

5.3. Cross-shore structure

There are no cross-shore transects from the low-wind period on June 7–10, 2005. However, an east–west transect line (Line C) was occupied for more than 26 h on June 13–14 during a time of persistent upwelling wind stress. The longitude of the line is 46.27°N, approximately 2 km north of the center of rotation found on the north–south line. Horner-Devine et al. (2008) examine data from the east–west line in more detail and show that bulge circulation is attenuated between ebb tides, presumably by the upwelling wind stress. As a result, the bulge circulation only appears after the ebb tide and is subsequently swept offshore and to the south. With these limitations in mind, two transects of north velocity from the east–west line are examined to determine the cross-shore structure of the plume (Fig. 7). In both transects the anticyclonic flow is clear, suggesting that even in moderate upwelling conditions, the estuarine outflow executes a rightward turn and generates a gyre.

The longitude of the center of rotation is estimated from the profiles in Fig. 7 to be approximately 124.29°E, or 18.2 km from the river mouth. This value is equivalent to the parameter y_c computed in the laboratory work of HD06, and describes the displacement of the center of rotation of the bulge from shore. The observed offshore distance of the bulge center is likely to be a lower bound on y_c since the upwelling wind stress destroys the circulation between tidal cycles and so the bulge never accumulates fluid for more than that period.

The longitude of the edge of the bulge circulation is 124.39°E, giving a radius of 8 km for the bulge and 4 km for the core circulation. Both of these values are significantly smaller than the equivalent values computed from the June 9–10 data (19 and 11 km, respectively). This may be due in part to the latitude of the center of rotation, which is expected to be further south during upwelling conditions than it was during the low-wind conditions. In this case, the east–west line may cross a narrower section of the bulge and cause the observed cross-shore scales to appear small. The radii are also expected to be smaller, however, since the bulge circulation is destroyed on each tidal cycle by the upwelling wind. In this case, the observed radii are interpreted as the

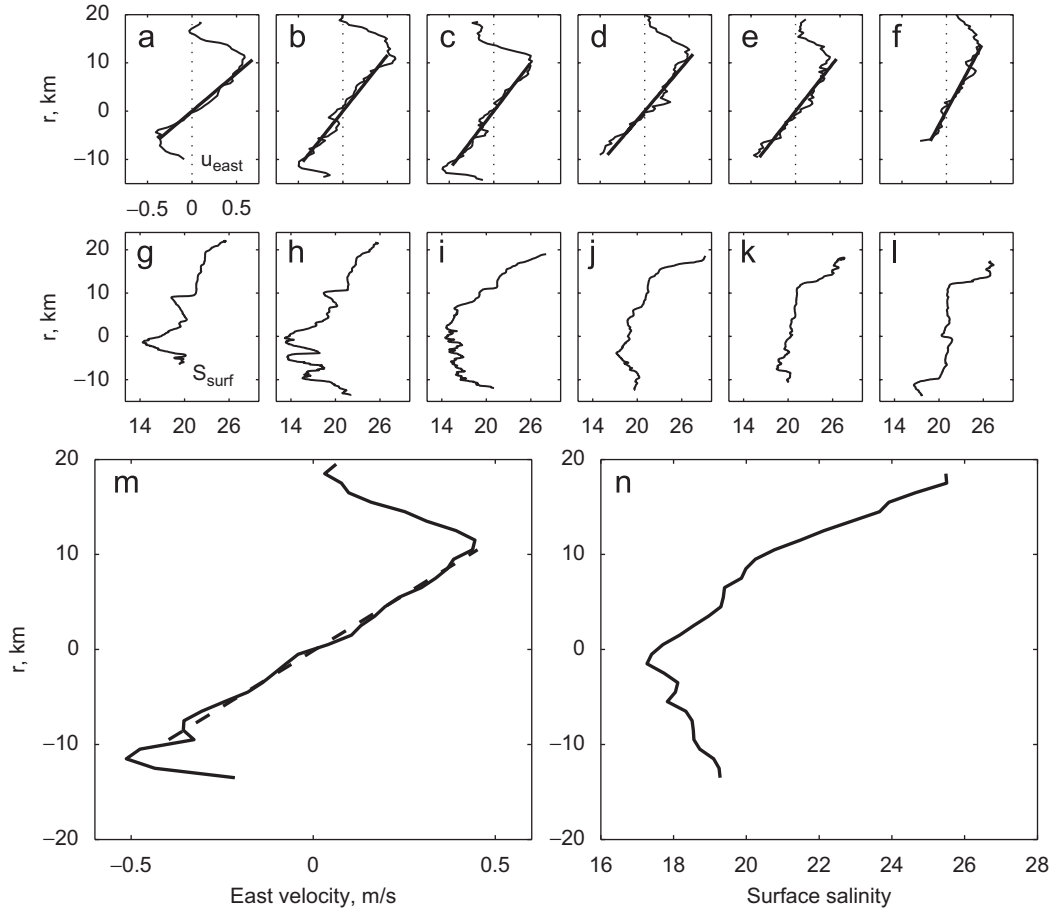

Fig. 6. Surface velocity and salinity in the bulge. (a)–(f) Surface profiles of east velocity plotted versus distance from the center of rotation (see Fig. 8(a)), (g)–(l) surface salinity profiles, (m) composite surface velocity profiles based on the data in (a)–(f), and (n) composite surface salinity profile based on the data in (g)–(l). Positive (negative) values of r correspond to points that are north (south) of the center of rotation.

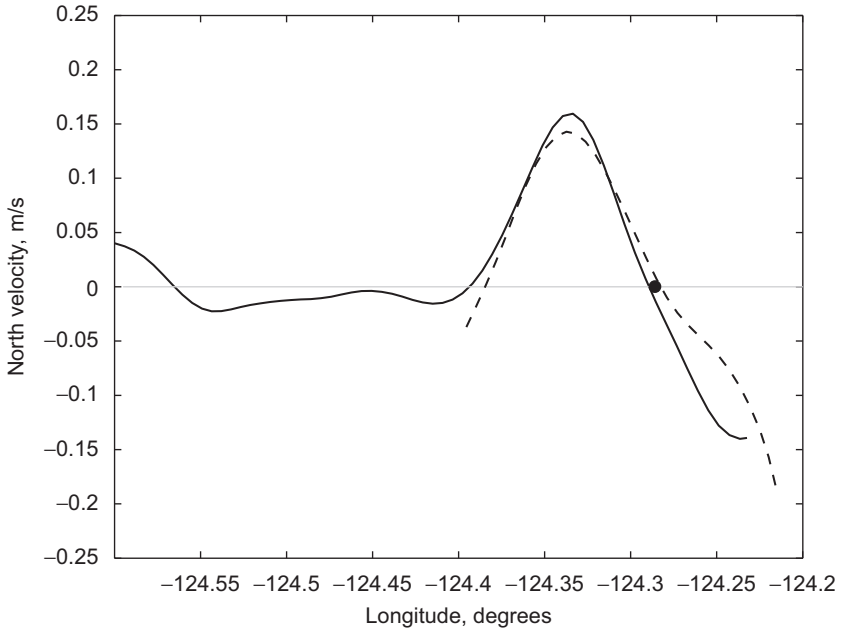

Fig. 7. North velocity (low-pass filtered) from two east–west transects on June 13, 2005. The latitude of the transect line is 46.27°N. The profiles were taken 11.1 (–) and 22.7 (- -) hours after high tide and both correspond to the beginning of the flood, when the lag is accounted for. The black dot is the estimate of the cross-shore center of rotation, which is approximately 18 km west of the river mouth at 124.05°E.

initial size of the bulge after it has been reset and before it has accumulated estuary discharge for more than one tidal cycle.

5.4. Temporal variability

The maximum azimuthal velocity, radius and vorticity derived from the surface velocity profile are plotted for each transect in Figs. 8b–d. For comparison, the tidal signal (Fig. 8e) has been shifted back by 3 h to account for the travel time necessary for the estuarine outflow to reach the transect location. Based on available estimates for the outflow velocity, this is a conservative estimate for the lag. After accounting for the lag, the first transect occurs during the latter half of the greater ebb, the fourth transect is centered on the lesser ebb, and the final transect occurs a few hours before the subsequent greater ebb (Fig. 8e).

Both the maximum azimuthal velocity and the average bulge radius are relatively constant throughout the sampling period, however, the velocity is highest and the radius smallest immediately after the maximum ebb outflow. The average velocity and radius are $0.5\,\mathrm{m\,s^{-1}}$ and 11 km, respectively. Here the radius is defined as half the distance between the velocity minima and maxima. This definition eliminates errors associated with locating the bulge center that may arise due to shelf tidal currents. However, it slightly underestimates the radius in the second half of the sampling period, which suggests that the radius may be close to constant after the greater ebb.

In cylindrical coordinates, the average vertical vorticity is given by

$$\omega_b = \frac{1}{r}\frac{\partial}{\partial r}(ru_\theta) = 2\gamma, \tag{15}$$

where $\gamma = \partial u_\theta/\partial r = \text{constant}$ is calculated from the linear fit to the velocity profile (see Figs. 6a–f). The vorticity normalized by f is plotted in Fig. 8c for each pass. It varies between $-1.25f$ and $-0.55f$ over the sampling period and has an average value of $-0.8f$, suggesting that the bulge is close to the zero potential vorticity limit. During the first transect, immediately following greater ebb, the vorticity exceeds f. This high vorticity value, which cannot be sustained in a rotational system due to inertial instability, suggests that the momentum from the estuary inflow exerts a dominant influence during this portion of the tidal cycle. The vorticity on either side of the inflowing jet was estimated to be $\pm 3f$ on a transect closer to the mouth (Horner-Devine et al., 2008). After the initial ebb pulse, the vorticity magnitude decreases, increases slightly on the lesser ebb and decreases again during the final flood. Although there are not enough data points to make this correlation with the tides rigorous, the data suggest that there may be some tidal variability in the bulge vorticity.

5.5. Momentum balance

Many of the terms in the radial momentum balance equation (Kundu, 1990):

$$\frac{\partial u_r}{\partial t} + u_r\frac{\partial u_r}{\partial r} + \frac{u_\theta}{r}\frac{\partial u_r}{\partial \theta} - \frac{u_\theta^2}{r} - fu_\theta = -g'\frac{\partial h}{\partial r} + \nu_e\left(\nabla^2 u_r - \frac{u_r}{r^2} - \frac{2}{r^2}\frac{\partial u_\theta}{\partial \theta}\right) \tag{16}$$

can be estimated with the density and velocity data from these transects. For ease of comparison with the acquired data, a single active layer form of the momentum equation

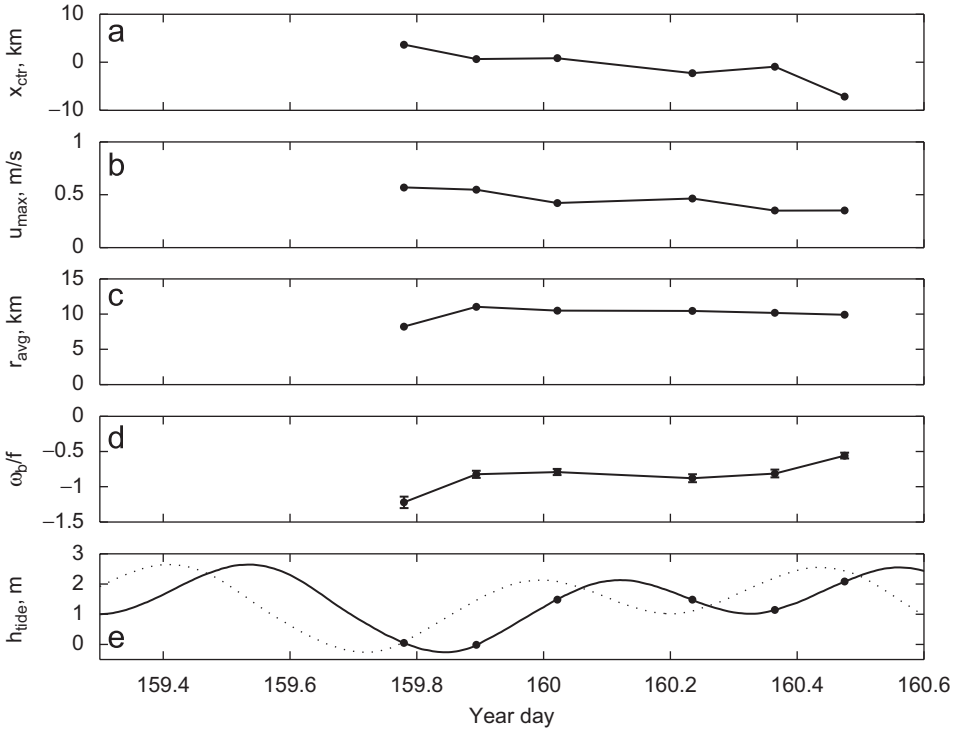

Fig. 8. Temporal variability of the bulge circulation. (a) Location of the bulge center north (positive) or south (negative) of its mean location. (b) Maximum eastward surface velocity for each transect. (c) Radius of core anticyclonic circulation, based on the distance from the location of maximum eastward velocity to that of the center of rotation. (d) Bulge vorticity normalized by the Coriolis frequency, f. The vorticity is derived from a linear fit to the surface velocity in the bulge core. (e) Tidal elevations at the mouth of the Columbia River (dotted line) and tidal elevations shifted by 3 h to account for the travel time between the mouth and the transect location (solid line). In each panel, dots correspond to the average time of each transect.

is considered in which vertical mixing is neglected. We compute the momentum balance terms based on Transect 3, which is least affected by the propagation of the tidal plume and the ensuing train of solitons.

Azimuthal and radial surface velocity profiles u_θ and u_r are vertically averaged over the upper water column as in Section 5.2 and low-pass filtered with a second order Butterworth filter (Figs. 9a and b). As was done previously, the radial coordinate, r, is defined relative to the center of rotation, which is determined from a linear fit to the core bulge circulation. The plume thickness, h, is determined based on the $S = 26$ isohaline and fit with a second order polynomial (Fig. 9c). The thickness gradient, $\mathrm{d}h/\mathrm{d}r$, is computed directly from the coefficients of the polynomial fit and the pressure gradient term is subsequently estimated using the value of the reduced gravity from Section 5.1, $g' = 0.097\,\mathrm{m\,s^{-2}}$.

The three terms in the gradient-wind balance (Eq. (2)) are plotted in Fig. 9d, and the error, $fu_\theta + u_\theta^2/r - g'(\mathrm{d}h/\mathrm{d}r)$, is plotted in Fig. 9e. It is clear that all three terms are significant in the momentum balance. The average error is 10% of the maximum value of the Coriolis term in the core region of the bulge. This confirmation of the gradient-wind balance is in good agreement with the laboratory results of HD06 and the prior assumptions of Yankovsky and Chapman (1997). It also validates the same assumption in the model proposed in Section 3.

In order to further verify the gradient-wind balance, the remaining terms in Eq. (16) are estimated, although some estimates are crude due to data limitations (Fig. 9f). These terms are referred to as the error terms since they represent the error when a gradient-wind balance is assumed. In Fig. 9, $\partial u_r/\partial t$, $u_r(\partial u_r/\partial r)$, and $v_e\nabla^2 u_r$ are plotted. Two viscous terms are omitted from this calculation. $v_e(u_r/r^2)$ will have approximately the same magnitude as the Laplacian term and $v_e(2/r)(\partial u_\theta/\partial\theta)$ is expected to be small due to axial symmetry. A value of $v = 10\,\mathrm{m^2\,s^{-1}}$ was used for the lateral eddy diffusivity (e.g. Jones and Marshall, 1993), though the viscous term remains a secondary term even when a value two orders of magnitude higher is used. In estimating the magnitude of these terms, the time derivative is calculated based on the difference between the velocity data in transect three and four, which corresponds to $\Delta t = 5.1$ h. Although it is not feasible to directly estimate the angular derivative in $u_\theta/r(\partial u_r/\partial\theta)$, a crude estimate based on the difference between the northern and southern radial profiles ($\Delta\theta = \pi$) suggests that this term is also small and, thus, that the assumption of axial symmetry is reasonable.

The leading error term is the unsteady term, $\partial u_r/\partial t$, whose magnitude is approximately equal to the error in the gradient-wind equation (Figs. 9e and f). This estimate of the radial acceleration is higher than that predicted in Section 3. It is likely that the observed temporal variability

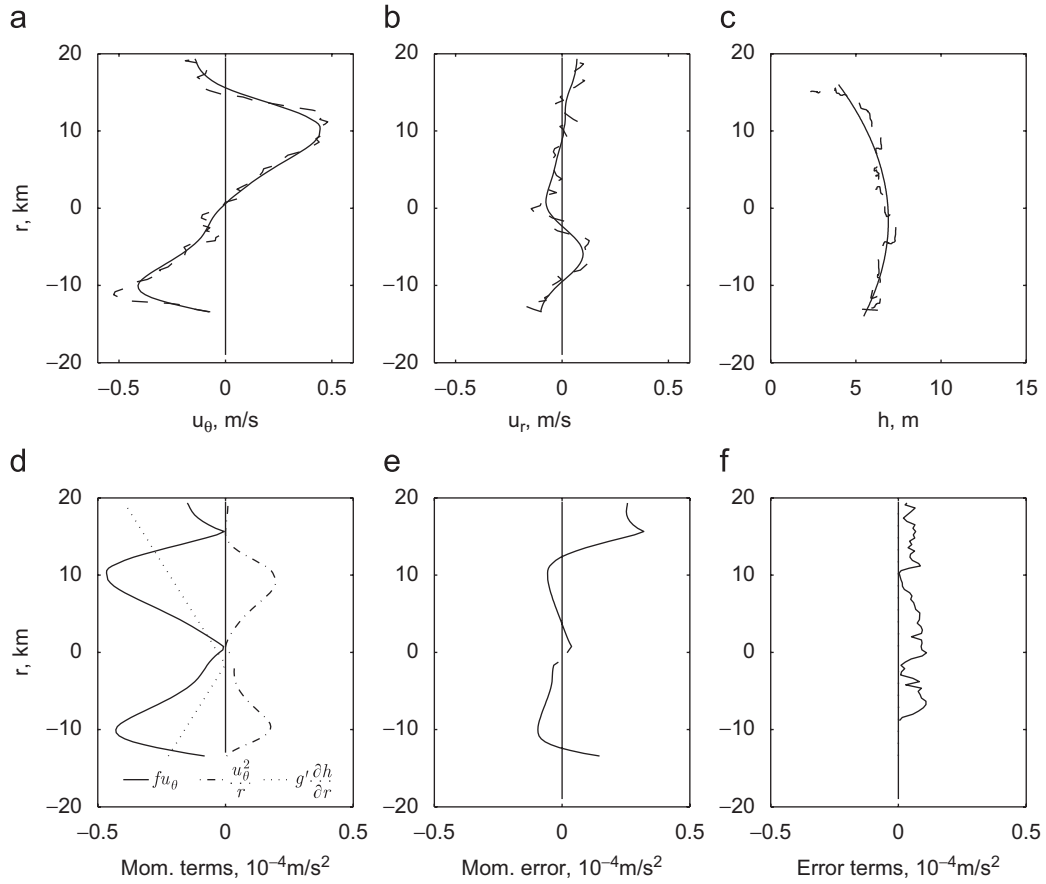

Fig. 9. Radial momentum balance based on Transect 3. (a) Azimuthal surface velocity (- -) and filtered (–). (b) Radial surface velocity (- -) and filtered (–). (c) $S = 26$ isohaline (- -) and quadratic fit (–). (d) Terms in the gradient-wind momentum balance. (e) Momentum balance error: $fu_\theta + u_\theta^2/r - g'(\mathrm{d}h/\mathrm{d}r)$. (f) Radial acceleration, $\partial u_r/\partial t$ (-). The remaining computed error terms ($u_r(\partial u_r/\partial r)$ and $v_e\nabla^2 u_r$) are plotted but are of a much smaller magnitude. In all panels, positive (negative) values of r correspond to points that are north (south) of the center of rotation.

is the result of changes in the wind stress or the tidal phase rather than the bulge growth.

6. Discussion

The results presented in Section 5 support a number of assumptions in existing models of the bulge circulation. As observed in prior laboratory studies (HD06), the vorticity is constant in the central region of the bulge. This observation, which is analogous to solid-body rotation, provides an important simplification for analytical models and allows other bulge parameters such as the center of rotation, radius, average vorticity and maximum velocity to be estimated reliably. The average vorticity in the bulge is found to be close to $-f$ and thus the assumption of zero potential vorticity in the bulge appears also to be a reasonable simplification for the Columbia plume. The fact that the bulge vorticity is close to $-f$ is a somewhat surprising result since the initial potential vorticity of an outflow is $-fH^{-1}$ and, thus, a zero potential vorticity flow is associated with a very deep outflow. In the case of the Columbia plume, however, the estuary discharge is shallow (5–10 m). A more detailed analysis of the potential vorticity dynamics is needed to resolve this interesting result.

The momentum balance in the bulge is confirmed to be in gradient-wind balance (Eq. (2)), a balance that is often assumed for the bulge, but has not been validated before this study. Finally, the freshwater volume in the bulge is estimated to be the equivalent of at least 3–4 days of river discharge. While the current study cannot directly measure the unsteady growth of the bulge due to the length of the sampling period, this result is consistent with the conclusion that the bulge accumulates a large fraction of the river discharge and thus reduces the northward freshwater transport in the coastal current. In the remainder of this section, the comparisons between the observations and previously developed theories are discussed and extended.

6.1. Comparison with theory

The theory that is presented in Section 3 makes two assumptions: the bulge circulation is in a gradient-wind momentum balance and the vorticity is spatially uniform in the bulge. Since both of these assumptions have been validated for the current data set, Eq. (5) is expected to be a good description of the bulge interface. Furthermore, since the bulge vorticity is close to $-f$, Eq. (6) is also expected to apply.

The theoretical interface profile corresponding to Eq. (5), the constant vorticity solution, is plotted with the observed salinity structure in Fig. 3a. For this comparison, observed values of $g' = 0.10\,\mathrm{m\,s^{-2}}$, $\omega_b/f = -0.8$ and $R = 20\,\mathrm{km}$ are used. It is important to note here that R is interpreted as the radius at which the interface surfaces, which also corresponds to the point where the velocity returns to zero. The assumptions of uniform vorticity and of a gradient-wind balance do not appear to be valid outside the core region, and thus may not apply in the region between the maximum velocity and the outer edge of the bulge circulation. The true radial velocity profile is more complicated than that implied by solid-body rotation and considered in this analysis. The profile may be better modeled as a Rankine vortex (e.g. Moulin and Flor, 2006), which consists of a core with constant vorticity and an outer region in which the velocity decays and the vorticity is approximately zero. Nonetheless, the computed profile approximates the observed profile well (Fig. 3a) in that the profile agrees well with the $S = 26$ contour, chosen independently as the plume base. From Eq. (5), the curvature and maximum depth of the interface profile are given by

$$\frac{\partial^2 h}{\partial r^2} = \frac{\omega_b\left(\frac{\omega_b}{2} + f\right)}{2g'}, \tag{17}$$

$$h_{\max} = -\frac{\omega_b\left(\frac{\omega_b}{2} + f\right)}{4g'} R^2. \tag{18}$$

Based on the observed values of g', ω_b and R, $\mathrm{d}^2h/\mathrm{d}r^2 = -3.3 \times 10^{-8}\,\mathrm{m^{-1}}$ and $h_{\max} = 6.58\,\mathrm{m}$. For comparison, the quadratic fit to the $S = 26$ contour computed in Section 5.5 resulted in a value for the curvature of $-1.9 \times 10^{-8}\,\mathrm{m^{-1}}$. While these are remarkably close considering the simplicity of the model, the theoretical profile over-predicts the actual curvature by approximately 40%. The maximum depth, however, compares well with the observed mean depth in the center of the bulge, $h_b = 6.61\,\mathrm{m}$. Since the predicted maximum depth is a function of R, which is assumed to grow in time, this prediction accounts for the deepening of the bulge as it accumulates estuary water. The zero potential vorticity solution is indistinguishable form the constant potential vorticity case plotted in Fig. 3a since the observed vorticity is close to $-f$.

The good agreement between the theoretical profile and the observations provides further support for the gradient-wind and constant vorticity assumptions. The model could be further improved with a more sophisticated treatment of the region between the maximum velocity and the outer edge of the bulge. However, the observations suggest that the current model is adequate and, further, that the assumption of zero potential vorticity is justified for the present case.

6.2. Bulge scales

The laboratory study of HD06 suggests that the bulge dynamics can be characterized in terms of two length scales: the bulge radius r_b and the displacement of the center of rotation from shore y_c. These scale with the internal deformation radius L_b and the inertial radius L_i, respectively. The ratio $L^* = L_i/L_b$ is a prediction of how closely the bulge circulation is pressed to the coast, as described in Section 2. The intention of these laboratory experiments was to describe the plume behavior in terms of parameters that are known *a priori*. In the case of the Columbia River plume, however, the correct *a priori* parameters are not clearly defined due to the strong influence of the tides and the estuary circulation. For example, the magnitude of the estuary discharge varies by more than a factor of four over the course of the tidal cycle.

The average river discharge during this period was $Q = 7000\,\mathrm{m^3\,s^{-1}}$ (Fig. 2b), the width and depth of the outflow are approximately $W = 3000\,\mathrm{m}$ and $H = 5\,\mathrm{m}$, respectively, and $g' = 0.2\,\mathrm{m\,s^{-2}}$. Based on these values, the average discharge velocity is $U = 0.5\,\mathrm{m\,s^{-1}}$. Using these parameters, we obtain the following (see Section 2 for definitions of these parameters):

$$Ro_i = 1.6, \quad Fr_i = 0.5, \quad L_b = 7.1\,\mathrm{km}, \quad L_i = 4.5\,\mathrm{km}, \quad h_b = 2.6\,\mathrm{m}. \tag{19}$$

Thus, the governing parameter $L^* = L_i/L_b = 0.6$, which is a moderately high value of L^* and suggests that the bulge circulation is expected to be relatively far from shore. For comparison, the observed bulge scales are $r_b = 20\,\mathrm{km}$ and $y_c = 18\,\mathrm{km}$. These are depicted in Fig. 10. Their ratio, $y_c/r_b = 0.9$, confirming that the bulge is displaced from shore relative to its radius.

In HD06, y_c and r_b increase continuously in time as the bulge grows, and scale with L_i and L_b, respectively. Based on the current observations, $y_c/L_i = 4$ and $r_b/L_b = 2.8$. These values correspond to 12 and 8 days after plume initiation in the laboratory experiments (see Figs. 6b and 7b in HD06). This duration of bulge growth is unlikely, as the plume experienced sustained upwelling winds 3–4 days prior to the June 9–10 observations, which are assumed to attenuate the bulge circulation. This suggests that the scales used to determine L_i and L_b may underestimate the actual bulge scales. This is not surprising due to the large tidal variability of the estuary discharge. The role of tides was not included in the experiments of HD06 and, thus, the effect on the expected plume scales presented in that study is not known. The effect of tides is complicated because it introduces variability on time scales shorter than the geostrophic time scales that are implicit in the scaling in HD06.

The estuary discharge during maximum ebb was measured during this study to be approximately $Q = 35{,}000\,\mathrm{m^3\,s^{-1}}$ (Horner-Devine et al., 2008), with $H = 8\,\mathrm{m}$. Assuming the same g', we obtain the following for the peak

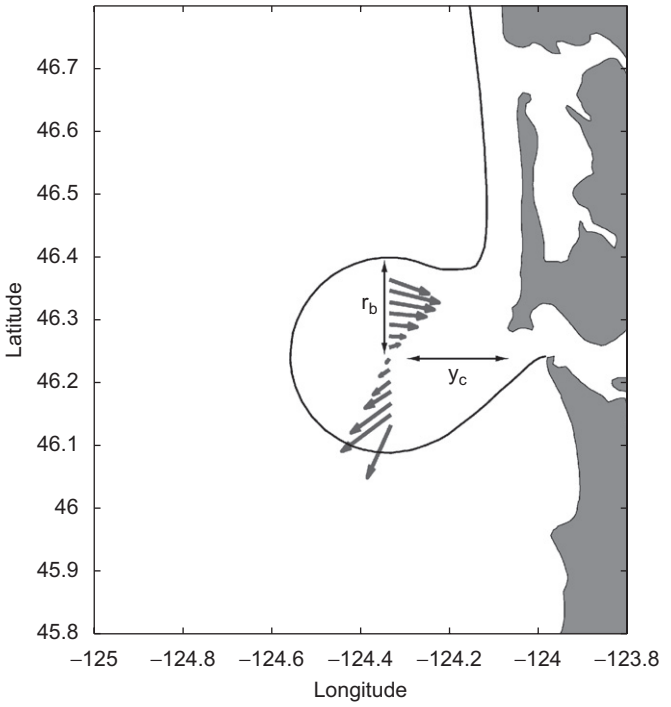

Fig. 10. Schematic of the Columbia River plume bulge based on the observed average velocity vectors (gray arrows). The approximate plume boundary has been drawn assuming that the bulge is circular. The scales y_c (= 18 km) and r_b (= 20 km), representing the displacement of the bulge from the coast and the radius of the bulge, respectively, have also been added.

ebb conditions:

$$Ro_i = 4.6, \quad Fr_i = 1.1, \quad L_i = 13.8\,\text{km}. \tag{20}$$

Based on the above scales, $y_c/L_i = 1.3$, which corresponds to approximately 1.5 days of accumulation when compared with the results in HD06. Although the scaling of HD06 cannot be directly applied to the tidal discharge, this result suggests that the massive ebb pulse may contribute to the shape of the bulge.

The tides appear to increase the cross-shore scale of the bulge above the expected average value for the same flow conditions, leading to an increase in L^* from 0.6 for the average conditions to 1.3 for the maximum ebb. In the experiments of HD06, the plume was observed to become unstable when $y_c/r_b > 0.7$, resulting in a bulge that alternately pinched off from and re-attached to the coast and pulsed coastal current transport. The observed value of y_c/r_b is well above this stability criterion, suggesting that the tides may cause the bulge to pinch off and the alongshore transport to be pulsed. This result is generally consistent with the conclusion drawn by Yankovsky et al. (2001), who show that periodic modulation of the river discharge causes pulses of buoyant fluid to be released in to the coastal current. However, Yankovsky et al. (2001) find that this modulation only occurs when the period of the river modulation exceeds the tidal period. This final conclusion and the predictions of this study are therefore in contradiction, but cannot be resolved in the present data set.

Yankovsky and Chapman (1997) develop an analytical prediction for the radius of the bulge in which they assume that the bulge is steady (i.e. the radius is constant) and is in a gradient-wind balance (Eq. (2)). In their analysis, the maximum azimuthal bulge velocity is found by applying Bernoulli's equation between the inflow and the outer edge of the bulge. With these assumptions, the bulge radius r_s is given by

$$r_s = \frac{(3g'h_0 + U^2)}{f(2g'h_0 + U^2)^{1/2}}, \tag{21}$$

where h_0 is the inflow thickness. Evaluating Eq. (21) using the average inflow parameters, the bulge radius is predicted to be 20.6 km. This agrees very well with the observed radius $r_b = 20$ km, despite the fact that Bernoulli's equation is unlikely to be valid due to the intense mixing observed near lift-off in the Columbia plume.

The above estimates for the bulge scale appear to be in contradiction, since the former assumes that the bulge is constantly growing in time and the latter assumes that it is steady. The observation that $r_b = 8$ km during upwelling conditions (Section 5.3), when the plume is assumed to be reset after each tide, provides circumstantial evidence that the bulge observed during low-wind conditions (r_b = 20 km) has grown substantially. In addition, the estimates of alongshore transport presented in Section 6.3, which are well below the average freshwater discharge, and the observed freshwater volume of the bulge, both confirm that the bulge accumulates river water and must be unsteady. However, the observed bulge radius after 3–4 days of low-wind is in very good agreement with the steady estimate. Taken together, these suggest that, while the bulge grows initially, its size may ultimately be limited, and its steady-state size is well-predicted by Eq. (21).

In Eq. (19) the estimate for the bulge depth scale, h_b, suggested by Avicola and Huq (2003) and HD06 is also calculated. In both sets of laboratory experiments, the observed bulge depth increases continuously as the bulge expands and is between 2.0 and $2.5h_b$ after 4 days. The measured estimates of the mean plume depth range from 6.6 to 10.2 m, or 2.5 to $3.9h_b$ (Fig. 5). It appears that the depth scale underestimates the actual plume depth, presumably due to the increased mixing in the natural plume relative to the laboratory studies cited above or to the elevated discharge during ebb tide.

6.3. Alongshore transport

A primary goal in understanding the dynamics of the plume bulge is to quantify the reduction in the alongshore transport of river water due to the accumulation in the bulge. Both Fong and Geyer (2002) and HD06 find that the flux of freshwater that accumulates in the bulge Q_b/Q depends on the inflow Rossby number, Ro_i. Results from

these two experimental data sets are synthesized in HD06 (their Fig. 18). Using the average inflow parameters from this study and the relationship in HD06 Fig. 18, $Ro_i = 1.6$ and $Q_b/Q = 0.65$. The predicted value for the freshwater coastal current flux, $Q_{fw}/Q = 1 - Q_b/Q = 0.35$. Thus, most of the river water is predicted to accumulate in the bulge and only 35% to flow north in the coastal current.

Nof and Pichevin (2001) present an analytical model of the bulge growth based on the mass and momentum budgets in a control volume surrounding the inflow region. In their model, the fractional accumulation of river water in a constant vorticity bulge is given by

$$\frac{Q_b}{Q} = \frac{2\alpha}{(1+2\alpha)}, \tag{22}$$

where $\alpha = -\omega_b/f$. In their derivation they assume that the vorticity is constant and that the bulge is in gradient-wind balance, as we have confirmed for the present data. Using an average value of $\alpha = 0.8$, Eq. (22) predicts that $Q_b/Q = 0.62$, and thus $Q_{fw}/Q = 0.38$, in good agreement with the prediction from HD06. For the zero potential vorticity case Nof and Pichevin (2001) find that $Q_{fw}/Q = 0.33$, which also agrees with the above estimates and with the earlier conclusion that the bulge vorticity is close to the zero potential vorticity limit.

As described in Section 4, the RISE program involved simultaneous sampling using two vessels; the R/V Pt Sur and the R/V Wecoma. On the morning of June 10, during the bulge sampling period, the R/V Wecoma made an east–west pass across the coastal current just north of the mouth of the Columbia River along latitude 46.4°N. Although the velocity data from this transect do not resolve the plume, four CTD casts do. A preliminary estimate of the northward freshwater flux can be made by assuming that the coastal current is geostrophic (Fong and Geyer, 2002):

$$Q_{fw} = \frac{\rho_0}{g\beta S_0}\frac{(g'h_0)^2}{3f}, \tag{23}$$

where the salinity and density are assumed to vary linearly in the plume, $\beta = 0.79\,\mathrm{kg\,m^{-3}\,psu^{-1}}$ and h_0 is the maximum depth of the current at the coast. Based on the CTD data (Hickey, pers. comm.), we estimate that $\rho_0 = 1026\,\mathrm{kg\,m^{-3}}$, $S_0 = 32\,\mathrm{psu}$, $g' = 0.07\,\mathrm{m\,s^{-2}}$ and $h_0 = 6.5\,\mathrm{m}$. With these values Eq. (23) gives $Q_{fw} = 2700\,\mathrm{m^3\,s^{-1}}$, or $Q_{fw}/Q \simeq 0.4$. This estimate is in very good agreement with the two predictions listed above based on HD06 and Nof and Pichevin (2001). It is important to note, however, that this estimate is relatively crude as it does not take into account the ambient alongshore flow. Thus, the degree of agreement with the predictions is probably somewhat fortuitous. Nonetheless, this estimate broadly supports the conclusion that 50% or more of the river discharge is trapped in the bulge during this period.

6.4. The role of the wind

Wind plays a very important role in the dynamics of the Columbia River plume, and has been deliberately ignored in the present analysis. As described in Hickey et al. (2005), the plume may tend northward, southwestward or both, depending on the direction, magnitude and persistence of the coastal wind stress. The present observations were intentionally carried out during a period when the wind stress was moderate, and are not intended to describe the plume dynamics during periods of elevated wind stress. Rather, they are chosen for comparison with analytical, numerical and laboratory models that do not include wind in their formulations.

The low-wind scenario can be thought of as the base case for the plume dynamics, upon which the effects of wind stress or variable river discharge should be added. The conclusion that less than 50% of the river water is transported northward in the coastal current will certainly be modified during downwelling winds, when a much higher fraction is transported north in the coastal current, or upwelling winds, when much less is transported north. Thus, a complete understanding of the transport in the plume depends on the transport in low-wind conditions, as described here, as well as a quantitative prediction of the transport under varying wind scenarios. As a first step in this direction, further work should address the minimum downwelling and upwelling wind stresses required to completely transport or completely block, respectively, the northward freshwater flux.

7. Summary

The observations and analyses in the present work are used to investigate the dynamics of the river plume bulge near the end of a 4 day period of moderate wind stress. Velocity and density fields from a series of north–south transects through the Columbia River plume are presented and compared with predictions of the radius, depth, aspect ratio and momentum balance from laboratory, numerical and analytical studies.

Throughout the observation period, a persistent anticyclonic circulation is observed offshore of the river mouth corresponding to a 5–10 m deep low-salinity lens. This lens contains the equivalent of 3–4 days of freshwater discharge from the estuary. The circulation consists of a core region, in which the azimuthal velocity varies linearly, and an outer region, in which the velocity decreases to zero. This velocity structure is in good agreement with that observed in laboratory studies and confirms the common assumption of constant vorticity in the core of the bulge. The terms in the radial momentum balance are estimated in this core region and found to be in gradient-wind balance. The observed vorticity in the bulge is close to $-f$ and implies that the bulge is close to the zero potential vorticity limit. A theoretical bottom profile based on the gradient-wind balance and a constant vorticity assumption is computed,

which is in good agreement with the observed bulge structure.

Based on average and tidal river mouth parameters, the bulge aspect ratio is expected to be high (high L^*). Consistent with this prediction, the bulge radius and the displacement of the center of rotation from shore are found to be $r_b = 20$ km and $y_c = 18$ km, respectively. Their ratio, $y_c/r_b = 0.9$, confirms that the bulge is displaced far from the shore relative to its radius. Due to the mechanics of the re-attachment point along the coast (Whitehead, 1985), this is associated with a relatively lower coastal current freshwater flux. The bulge radius is found to be much larger than either the Rossby radius L_b or inertial radius L_i based on average inflow parameters, suggesting that the bulge is accumulating river water, however, neither scale predicts the expected accumulation of fluid in the bulge well. The prediction is more in line with the observations when the limiting value L_i based on the maximum tidal inflow parameters are used. Despite the unsteady nature of the bulge, the steady-state scale for the bulge radius, r_s, suggested by Yankovsky and Chapman (1997) predicts the observed radius very well. This suggests that, while the bulge grows initially, its radius may ultimately be limited to r_s. If this is true, it remains to determine why r_s predicts the bulge scale after a few days of growth, when the derivation assumes no growth.

Finally, the bulge observations are used to predict the northward transport of freshwater in the coastal current. Based on inflow Rossby number scaling from prior laboratory and numerical results (HD06 and Fong and Geyer, 2002), $Q_{fw}/Q = 0.35$, which agrees well with the prediction using the analytical theory of Nof and Pichevin (2001) of $Q_{fw}/Q = 0.38$. These predictions are also in good agreement with a preliminary estimate of the observed transport of $Q_{fw}/Q = 0.4$. Together, these results predict that the Columbia plume transported less than half of the total river discharge northward in the coastal current during this low-wind period.

Acknowledgments

The author is very thankful for the encouragement and support of David Jay, who bears much responsibility for the author's involvement in this project. The author would also like to thank Emily Spahn who helped with the data acquisition and some of the analysis, Philip Orton, Jay Peterson, Keith Leffler, Jiayi Pan, who helped with the data acquisition and Barbara Hickey who leads the project. The author would also like to thank Ron L. Short of the R/V Pt Sur and Marine Technicians Stewart Lamberdin, Christina Courcier, and Ben Jokinen for their superb support of in-situ data collection. Finally, MODIS and radar remote sensing data were kindly provided by Raphael Kudela and Mike Kosro, respectively. The research was supported by NSF OCE 0648655 and OCE 0239072 (River Influences on Shelf Ecosystems). This is RISE contribution number 18.

References

Avicola, G., Huq, P., 2003. The characteristics of the recirculating bulge region in coastal buoyant outflows. Journal of Marine Research 61, 435–463.

Chant, R., Glenn, S., Hunter, E., Kohut, J., Chen, R., Houghton, R., Bosch, J., Schofield, O., 2008. Bulge formation of a buoyant river outflow. Journal of Geophysical Research 113, C01017, doi:10.1029/2007JC004100.

Chao, S.-Y., Boicourt, B., 1986. Onset of estuary plumes. Journal of Physical Oceanography 16 (12), 2137–2149.

Flierl, G., 1979. A simple model for the structure of warm and cold core rings. Journal of Geophysical Research 84 (C2), 781–785.

Fong, D., Geyer, W., 2002. The alongshore transport of fresh water in a surface-trapped river plume. Journal of Physical Oceanography 32 (3), 957–972.

Garvine, R., 1987. Estuary plumes and fronts in shelf waters: a layer model. Journal of Physical Oceanography 17 (11), 1877–1896.

Garvine, R., 2001. The impact of model configuration in studies of buoyant coastal discharge. Journal of Marine Research 59, 193–225.

Hickey, B., Peitrafesa, L., Jay, D., Boicourt, W., 1998. The Columbia River plume study: subtidal variability in the velocity and salinity field. Journal of Geophysical Research 103 (C5), 10339–10368.

Hickey, B., Geier, S., Kachel, N., MacFadyen, A.F., 2005. A bi-directional river plume: the Columbia in summer. Continental Shelf Research 25 (14), 1631–1656.

Horner-Devine, A., Fong, D., Monismith, S., Maxworthy, T., 2006. Laboratory experiments simulating a coastal river inflow. Journal of Fluid Mechanics 555, 203–232.

Horner-Devine, A., Jay, D., Orton, P., Spahn, E., 2008. A conceptual model of the strongly tidal Columbia River plume. Journal of Marine Systems, accepted.

Jickells, T.D., 1998. Nutrient biogeochemistry of the coastal zone. Science 281 (5374), 217–222.

Jones, H., Marshall, J., 1993. Convection with rotation in a neutral ocean—a study of open-ocean deep convection. Journal of Physical Oceanography 23 (6), 1009–1039.

Kourafalou, V., Oey, L., Wang, J., Lee, T., 1996. The fate of river discharge on the continental shelf: part 1. Modeling the river plume and the inner shelf coastal current. Journal of Geophysical Research 101 (C2), 3415–3434.

Kudela, R., Peterson, T., Roberts, A., 2006. The role of river plumes in controlling phytoplankton productivity on the Oregon/Washington shelf. Eos Transactions AGU 87 (36).

Kundu, P.K., 1990. Fluid Mechanics. Academic Press, New York.

Moulin, F.Y., Flor, J.B., 2006. Vortex-wave interaction in a rotating stratified fluid: WKB simulations. Journal of Fluid Mechanics 563, 199–222.

Nash, J.D., Moum, J.N., 2005. River plumes as a source of large-amplitude internal waves in the coastal ocean. Nature 437 (7057), 400–403.

Nof, D., 1981. On the dynamics of equatorial outflows with application to the amazons basin. Journal of Marine Research 39 (1), 1–29.

Nof, D., 1988. Eddy-wall interactions. Journal of Marine Research 46 (3), 527–555.

Nof, D., Pichevin, T., 2001. The ballooning of outflows. Journal of Physical Oceanography 31 (10), 3045–3058.

Oey, L., Mellor, G., 1993. Subtidal variability of estuarine outflow, plume and coastal current: a model study. Journal of Physical Oceanography 23 (1), 164–171.

Orton, P.M., Jay, D.A., 2005. Observations at the tidal plume front of a high-volume river outflow. Geophysical Research Letters 32 (11).

Pichevin, T., Nof, D., 1997. The momentum imbalance paradox. Tellus 48A (2), 298–319.

Schofield, O., Chant, R., Glenn, S., Chen, R., Bosch, J., Gong, D., Kahl, A., Kohut, J., Hunter, E., Moline, M., Oliver, M., Reinfelder, J., Frazer, T., 2007. The hudson river plume and its role in low dissolved oxygen on the mid-Atlantic bight. Journal of Geophysical Research, submitted for publication.

Thomas, A.C., Weatherbee, R.A., 2006. Satellite-measured temporal variability of the Columbia River plume. Remote Sensing of Environment 100 (2), 167–178 iSI Document Delivery No.: 009MG Times Cited: 0 Cited Reference Count: 16.

Whitehead, J., 1985. The deflection of a baroclinic jet by a wall in a rotating fluid. Journal of Fluid Mechanics 157, 79–93.

Yankovsky, A., Chapman, D., 1997. A simple theory for the fate of buoyant coastal discharges. Journal of Physical Oceanography 27 (7), 1386–1401.

Yankovsky, A.E., Hickey, B.M., Munchow, A.K., 2001. Impact of variable inflow on the dynamics of a coastal buoyant plume. Journal of Geophysical Research-Oceans 106 (C9), 19809–19824.